Analysis of individual cone-photoreceptor directionality using scanning laser ophthalmoscopy

Diego Rativa* and Brian Vohnsen

Advanced Optical Imaging Group School of Physics, University College Dublin, Dublin 4, Ireland

**diego-jose.rativa-millan@ucd.ie*

http://www.ucd.ie/advancedopticalimaging/

Abstract: Scanning laser ophthalmoscopy has been used to measure individual cone-photoreceptor directionalities in the living human eye. The directionality is determined at different retinal eccentricities where it is expected that cones have diameters ranging between 5-10μm, comparable to the spot size of the incident beam. Individual cone directionality values are compared with the predicted directionalities obtained by using the waveguide model of light coupling to and from photoreceptors for the case of a focused incident beam.

OCIS codes: (330.7331) Visual optics, receptor optics; (330.7327) Visual optics, ophthalmic instrumentation.

References and links

1. W. S. Stiles and B. H. Crawford, "The luminous efficiency of rays entering the eye pupil at different points," Proc. R. Soc. London, Ser. B **112**, 428–450 (1933).
2. G. Toraldo di Francia and L. Ronchi, "Directional scattering of light by the human retina," J. Opt. Soc. Am. **42,** 782–783 (1952).
3. J. M. Enoch, "Optical properties of the retinal receptors," J. Opt. Soc. Am. **53,** 71–85 (1963).
4. A. W. Snyder and C. Pask, "The Stiles-Crawford effect explanation and consequences," Vision Res. **13,** 1115–1137 (1973).
5. A. Roorda and D. R. Williams, "Optical fiber properties of individual human cones," J. Vision **2**, 404–412 (2002).
6. B. Vohnsen and D. Rativa, "Absence of an integrated Stiles-Crawford function for coherent light," J. Vision **11**, 1–10 (2011).
7. B. Vohnsen, I. Iglesias, and P. Artal, "Guided light and diffraction model of human-eye photoreceptors," J. Opt. Soc. Am. A **22,** 2318-2328 (2005).
8. D. Rativa and B.Vohnsen, "Simulating human photoreceptor optics using a liquid-filled photonic crystal fiber," Biomed. Opt. Express **2**, 543–551 (2011).
9. J. M. Enoch and G. M. Hope, "Directional sensitivity of the foveal and parafoveal retina," Invest. Ophthalmol. Visual Sci. **12**, 497–503 (1973).
10. J. M. Gorrand and F. C. Delori, "A method for assessing the photoreceptor directionality," Invest. Ophthalmol. Visual Sci. **31** (suppl.), 425 (1990).
11. J. M. Gorrand and F. C. Delori, "A reflectometric technique for assessing photoreceptor alignment," Vision Res. **3**, 990–1010 (1995).
12. P. J. Delint, T. T. J. M. Berendschot, and D. van Norren, "Local photoreceptor alignment measured with a scanning laser ophthalmoscope," Vision Res. **37,** 243–248 (1997).
13. S. A. Burns, S. Wu, F. C. Delori, and A. E. Elsner, "Direct measurement of human cone-photoreceptor alignment," J. Opt. Soc. Am. A **12,** 2329-2338 (1996).
14. W. Gao, B. Cense, Y. Zhang, R. S. Jonnal, and D. T. Miller, "Measuring retinal contributions to the optical Stiles-Crawford effect with optical coherence tomography," Opt. Express **16,** 6486–6501 (2008).

#143458 - $15.00 USD Received 1 Mar 2011; revised 21 Apr 2011; accepted 27 Apr 2011; published 4 May 2011

15. W. Gao, R. S. Jonnal, B. Cense, O.P. Kocaoglu, Q. Wang, and D. T. Miller, "Measuring directionality of the retinal reflection with a Shack-Hartmann wavefront sensor," Opt. Express **17,** 23085–23097 (2009).
16. C. A. Curcio, K. R. Sloan, R. E. Kalina, and A. E. Hendrickson, "Human photoreceptor topography," J. Comp. Neurol. **292**, 497–523 (1990).
17. B. Vohnsen and D. Rativa, "Ultrasmall spot size scanning laser ophthalmoscopy," Biomed. Opt. Express. Submitted.
18. H. Hofer, P. Artal, B. Singer, J. L. Aragon, and D. R. Williams, "Dynamics of the eyes wave aberration," J. Opt. Soc. Am. A **18,** 497-506 (2000).
19. A. Ghatak and K. Thyagarajan, "Introduction to fiber optics," (Cambridge, U.K., 1998), pp. 149-156.
20. D. Marcuse, "Loss analysis of single-mode fiber splices," Bell Syst. Tech. J. 56, **56**, 703–718 (1977).
21. J. M. Gorrand, M. Doly, and F. Bacin, "Macular pigment density assessed by directional fundus reflectance," J. Opt. Soc. Am. A **26,** 1847-1854 (2009).
22. S. A. Burns, S. Wu, J. Chang, and A. E. Elsner, "Variations in photoreceptor directionality across the central retina," J. Opt. Soc. Am. A **14,** 2033-2040 (1997).
23. G. Westheimer, "Dependence of the magnitude of the Stiles-Crawford effect on retinal location," J. Physiol. (London) **192**, 309–315 (1967).
24. J. A. Van Loo and J. M. Enoch, "The scotopic Stiles-Crawford effect," Vision Res. **15,** 1005–1009 (1975).
25. B. Lochocki, D. Rativa, and B. Vohnsen, "Spatial and spectral characterisation of the first and second Stiles-Crawford effects using tuneable liquid-crystal filters," J. Mod. Opt. (in press).

1. Introduction

The human eye is directionally sensitive as demonstrated by the Stiles-Crawford effect (SCE) [1] seen as a dramatic reduction in visibility of a light beam impinging the eye pupil towards its rim. The directionality also manifests itself in light reflected off the retina in what is referred to as the Optical Stiles-Crawford effect (OSCE) [2]. The SCE and OSCE are normally fitted to a Gaussian function at the pupil plane given by [1]:

$$\eta = 10^{-\rho(r-r_0)^2} \tag{1}$$

where r is a point within the pupil, r_0 is peak position of the intensity distribution and ρ is the coefficient of directionality that measures the width of the pupil apodization.

The SCE and the OSCE are related to the waveguide properties of the cones and their directionality selective mechanisms [3]. A well-accepted model of the ideal waveguide cone described by Snyder and Pask [4] assumes that the SCE is created by individual cone waveguide effects, where the light coupling and its consequences for the apodization effect at the pupil are collective contributions of individual cone effects. It has been experimentally observed that optical fiber properties of an ensemble of cones resemble those of an individual cone [5] and that the photoreceptors are sensitive to the slope of the wavefront incident on the retina [6] as expected on account of the SCE model.

Vohnsen et al. [7] have upgraded the waveguide model introducing the diffraction properties of light to and from photoreceptors. Unlike a ray-optic geometrical approach, the diffraction model is needed to analyze the directionality and indeed an analytic ρ may be found including the cases of focused and non-focused illumination on the retina [7]. Actually, for a focused beam of light, the directionality turns out to be highly dependent on the ratio between the spot size of the incident light and the size of the mode propagated along the photoreceptor. The model has been examined experimentally using a microstructure fiber bundle to simulate the retina cone mosaic [8].

Different techniques have been implemented to measure directionality of cones using psychophysical and reflectance measurements. In the original Stiles-Crawford setup [1] and posterior variations as introduced by Enoch & Hope [9], the entrance beam angle is changed while the subject compares the reduction in visibility with that of a reference beam entering the eye at the pupil point of maximum visibility. Gorrand & Delori [10, 11] have developed a photoreceptor alignment reflectometer that determines photoreceptor alignment by measuring the distribu-

#143458 - $15.00 USD Received 1 Mar 2011; revised 21 Apr 2011; accepted 27 Apr 2011; published 4 May 2011

tion of reflected light in the pupil. Delint et al. [12] introduced scanning laser ophthalmoscopy to measure local directionality in areas larger than 2×2deg (i.e. $\approx 0.5\times0.5$mm). In both of these reflection techniques, two apertures are used to simultaneously alter the angle of the entrance and exit beam, scanning the subject's pupil. Burns et al. have modified the Gorrand and Delori setup avoiding to stop the exit beam at the pupil permitting an image of the entire distribution of light backscattered by the retina [13]. Gao et al. have explored optical coherence tomography to measure directionalities at different major layers of the retina [14], and posteriorly have implemented the Hartmann-Shack wavefront sensor to distinguish the guided (directional) and the diffused (non-directional) components of the reflected light from the retina [15]. Exploring the gain of resolution that adaptive optics provides, Roorda & Williams have measured individual human cone directionalities using a fundus camera for a retinal region 1° nasal from the fovea [5].

Here, individual-human cone directionality measurements carried out with a scanning laser ophthalmoscope (SLO) are presented. The directionality coefficients are obtained at different superior parafoveal eccentricities of the authors's right eyes where the size of the cones are expected to increase from approximately 2.5μm to $\sim10\mu$m at 1° to 20° from the fovea, respectively [16]. The values are analyzed with the model of light coupling to and from photoreceptors considering an incident spot size of $w_r \approx 5.2\mu$m (i.e., a 10.4μm beam waist). The individual directionalities are compared with the corresponding collective values and directionality values obtained in previous studies.

2. Experimental method

Retinal images are acquired at a frame rate of 47fps (frame resolution of 512×490 pixels) using a non-commercial SLO. The SLO contains vertical and horizontal scanning mirrors located at conjugated planes of the subject's pupil (P), a ($2\times$) beam expander, and an adaptive optics system (reducing the total optical aberrations to a maximum remnant RMS wavefront error of approximately $\lambda/4$). Experimental details about the SLO system are contained in Ref. [17].

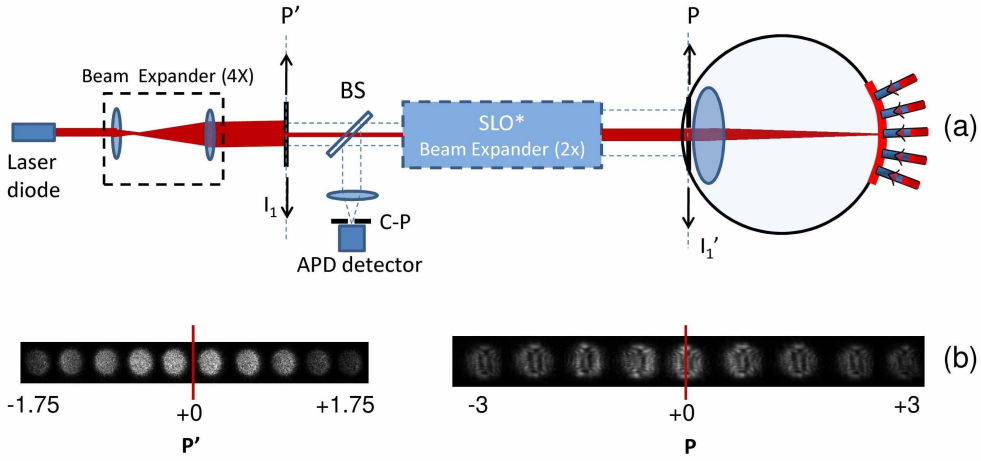

Fig. 1. Experimental method. (a) Experimental setup and (b) CCD images of the beam profile at the conjugated (P') and subject's (P) pupil position. * Further details about the SLO are given in Ref. [17].

As represented in Fig. 1, a laser diode at 785 nm wavelength (and 1 nm bandwidth) has been used as source. A laser diode was chosen for convenience as it was already present in our laboratory and in use for a related study [17], although to reduce unwanted interference effects

#143458 - $15.00 USD Received 1 Mar 2011; revised 21 Apr 2011; accepted 27 Apr 2011; published 4 May 2011

a superluminescent diode would be preferable. Nonetheless, the images and videos obtained (Section 4) do confirmatively show that cones have been resolved. An aperture I_1 with diameter of $\sim$ 0.8mm is translated 3.5mm through the conjugated pupil's plane (P') by using a motorized stage, corresponding to a movable artificial pupil (I_1') of $\sim$ 1.6mm translated 7mm across the plane of the subject's pupil. A beam splitter (BS) is used to select a part of the reflected light which is filtered by a confocal pinhole (C-P) and detected by an avalanche photodiode (APD). 100 image frames are collected simultaneously with the motorized transversal of 7mm of the incident illumination. Thus, between each image frame the incident beam has been displaced 70μm corresponding to a full scan of the subject's pupil in a lapse time of 2 seconds.

As shown in Fig. 1(b) the aperture scan through the laser introduces a Gaussian intensity-profile, where 0.9 mW (r=0) and 0.3mW (r=+3.5mm) are the maximum and minimum incident powers at the subject's pupil. The Gaussian profile of the laser has been characterized at the pupil plane in steps of 0.1mm and the Gaussian fitting-curve parameters are used to correct the reflection intensity in the videos such that the illumination corresponds to an intensity-constant artificial pupil. Figure 4(b) (Media 3) shows an example of an unprocessed and processed pair of videos, i.e., without and with correction of the beam intensity variations.

The right eye of both authors (DR: age 30 and BV:41, both with normal vision) has been examined with the dilated pupil ($\approx$ 8mm size, applying tropicamide 1%). A fixation target (Green LED) was used to set the viewing angle respectively at 2.5°, 5°, 10°, 15° and 20° superior thereby probing the superior parafoveal retina. Ethical approval for the research was obtained from the UCD Human Research Ethics Committee.

The directionality values are obtained acquiring the intensity values within the selected area (using ImageJ software) in steps of 0.35mm (i.e. every 5 frames) through the pupil scan (corresponding to 20 experimental points), obtaining an accurate fit of the apodization effect by using Eq. (1). Under unparalyzed accommodation conditions and during a time-lapse of 2 seconds there are maximum RMS wave-front error variations of $\sigma \sim$0.02μm with random characteristics [18], corresponding to a random Strehl ratio variations of ΔS=0.02. Thus, it is expected that in our case with a paralyzed accommodation condition, wave-front variations cannot alter significantly the Gaussian apodization of the reflection intensity during the scan of the subject's pupil.

3. Waveguide model of light coupling [7]

As represented in Fig. 2, the light guided in the cone is propagated from the inner to the outer segments where it is reflected by backscattering processes. Posteriorly, the light is guided back predominantly axially with single-mode characteristics (Gaussian shape), diffracted at the exit of the photoreceptor, and creating a Gaussian intensity distribution at the subject's pupil. For the case of an SLO system a focused beam is used to scan the subject's retina, in our experiment the estimated spot size at the retina is $w_r \approx 5.2\mu$m for an aperture of I_1' $\sim$ 1.6mm at the pupil. The incident beam intersects the photoreceptor at an angle $\theta = r/f_{eye}$ where part of the light is coupled to discrete modes as governed by waveguide boundary conditions. The fraction of power transmitted to the photoreceptor if incident with its peak value at the photoreceptor axis can be estimated from [19]:

$$T(\theta) = \left[\frac{2w_r w_m}{w_r^2 + w_m^2}\right]^2 exp\left[\frac{-2(\pi n_{eye} w_r w_m)^2 \theta^2}{\lambda^2 (w_r^2 + w_m^2)}\right] \quad (2)$$

where w_m is the width of the mode propagated. The eye parameters used are those of the schematic eye, i.e., a focal length f_{eye}=22.2mm and a constant index of refraction n_{eye}=1.33.

Assuming that the light intensity reflected by the photoreceptors towards the pupil [Eq. (1)] is linearly related to the amount of coupled incident light (i.e. bleached or constant fraction of

#143458 - $15.00 USD Received 1 Mar 2011; revised 21 Apr 2011; accepted 27 Apr 2011; published 4 May 2011

absorption) a directionality coefficient can be inferred directly from Eq. (2). as:

$$\rho(w_r, w_m) = 2\log(e)\left(\frac{\pi n_{eye}}{\lambda f_{eye}}\right)^2\left(\frac{w_r^2 w_m^2}{w_r^2 + w_m^2}\right) \tag{3}$$

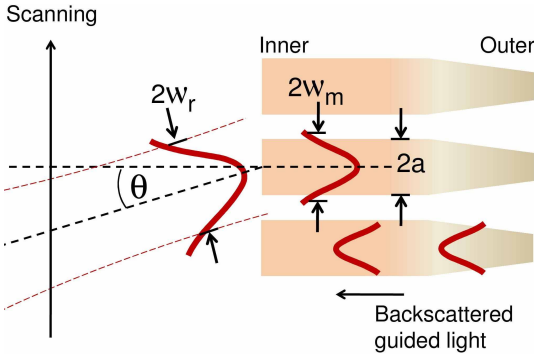

Fig. 2. Schematic of light coupling to the cone-photoreceptors at the retina plane for an SLO system.

Because of the small size of the outer segment and the scattering mechanisms within the cone it is expected that only the fundamental mode of the waveguide is guided back [7]. For a single-mode condition the mode-width is related to the radius of the waveguide (i.e. the photoreceptor radius, a) given by the empirical relation [20]:

$$a \approx w_m\left(0.65 + \frac{1.619}{V^{3/2}} + \frac{2.879}{V^6}\right)^{-1} \tag{4}$$

where V is the waveguide parameter. In Fig. 3 the dependence of the directionality coefficient with the photoreceptor size is estimated for different incident spot-size conditions and a waveguide parameter of V=2.0 by use of Eq. (3) and Eq. (4) [8].

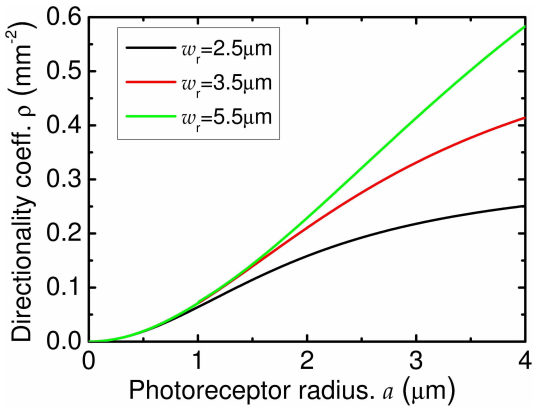

Fig. 3. Dependence of the predicted directionality coefficient with the photoreceptor size. The values are estimated for an illumination spot-size of w_r= 2.5μm, 3.5μm and 5.5μm .

Due to the scanning, only an area given by the spot size of the illumination beam (in our case approximately 1-3 cones) is illuminated simultaneously at any given instant and possible

#143458 - $15.00 USD Received 1 Mar 2011; revised 21 Apr 2011; accepted 27 Apr 2011; published 4 May 2011

collective effects as scattering created by a distribution of cones is avoided. This is under the assumption that multiple scattering may be ignored, which appears reasonable considering the low contrast of refractive indices within the retina whereby the illumination is dominated by the focused incident beam.

4. Results and discussion

In virtue of the small size of the cones in the central region, an individual cone analysis is not well-controlled, limited by the resolution of the image, and instead average values of selected areas are determined. Figure 4(a) (Media 1) and Fig. 5(a) (Media 6) show the directionality values obtained in areas selected at a distance of 0.65°, 1° and 1.5° from the center of the fovea for both subjects.

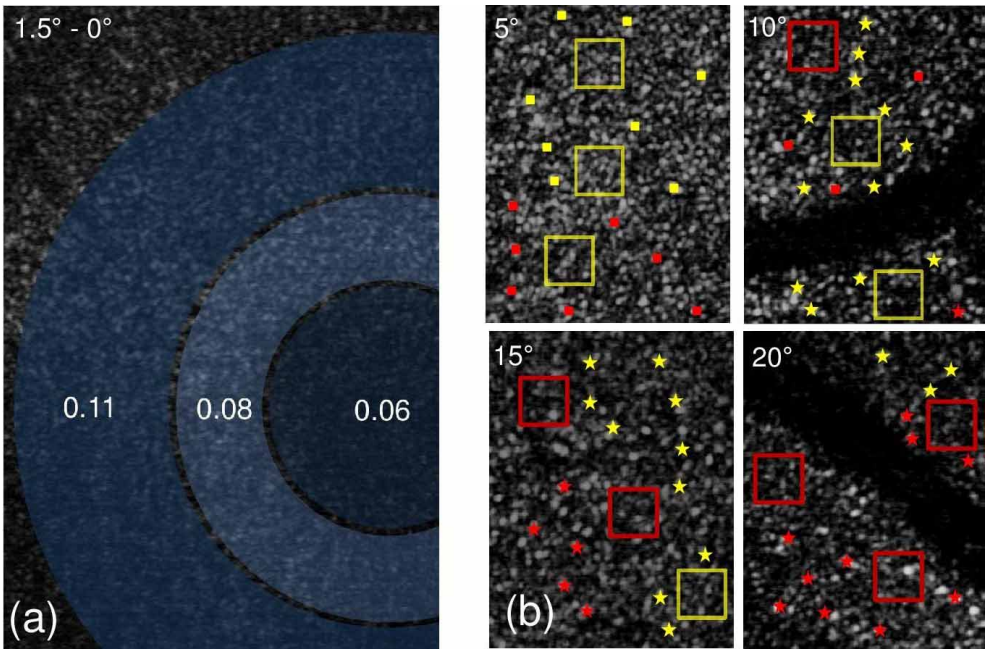

Fig. 4. Retinal images of the subject BV and directionality values at different retinal regions: (a) eccentricity from 0° to 1.5° (Media 1), the blue zones are the areas selected to measure the averaged value of directionality, the directionality coefficient of the areas selected is given in mm^{-2} units; (b) superior retinal eccentricities of 5° (Media 2), 10°* (Media 3), 15°(Media 4), and 20° (Media 5). The individual directionality values are represented by: (Yellow box) ρ= 0.10 - 0.15mm^{-2}, (Red box) ρ= 0.15 - 0.20mm^{-2}, (Yellow star) ρ= 0.20 - 0.30mm^{-2}, (Red star) $\rho > 0.30mm^{-2}$. The opened square represents the area selected to calculate the directionality averaged values with (Yellow square) ρ= 0.10 - 0.15mm^{-2} and (Red square) ρ= 0.15 - 0.20mm^{-2}. * The media shows a processed (intensity-constant artificial pupil) (a) and an unprocessed (uncorrected for the Gaussian laser beam profile) video (b).

Taking into account the radial eccentricity dependence of the cone-size [16], a ring-shape for the area selection has been adopted to analyze the directionalities. The highlighted blue regions are the areas selected for the analysis, a histogram furnish the mean intensity of the pixels in the area for each frame using an ImageJ application. Software-tracking and averaging of frames have been avoided, providing non-altered intensity values of reflection. Near the fovea there is

#143458 - $15.00 USD Received 1 Mar 2011; revised 21 Apr 2011; accepted 27 Apr 2011; published 4 May 2011

a brighter zone that follows the scan of the pupil caused by reflection at the inner limiting membrane [21]. It has a little impact, however, on the Gaussian shape of the apodization effect. The same effect cannot be seen for the parafoveal regions due to the changed direction of gaze.

As shown in Fig. 4(a) and Fig. 5(a) the increase of the directionality with the eccentricity resembles the dependence reported by Burns et al. [22] for OSCE directionality measurements, and the values reported by Westheimer [23] and Enoch & Hope [9] for the SCE measurements.

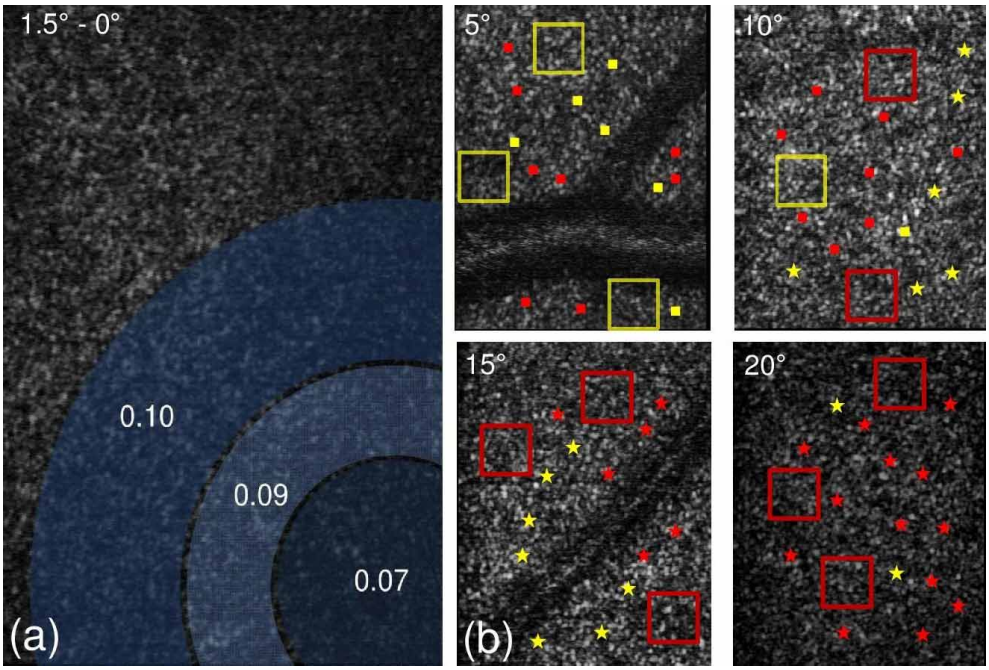

Fig. 5. Retinal images of the subject DR and directionality values at different retinal regions: (a) eccentricity from 0° to 1.5° (Media 6), the blue zones are the areas selected to measure the averaged value of directionality, the directionality coefficient of the areas selected is given in mm^{-2} units; (b) superior retinal eccentricities of 5° (Media 7), 10° (Media 8), 15°(Media 9), and 20° (Media 10). The individual directionality values are represented by: (Yellow box) ρ= 0.10 - 0.15mm^{-2}, (Red box) ρ= 0.15 - 0.20mm^{-2}, (Yellow star) ρ= 0.20 - 0.30mm^{-2}, (Red star) $\rho > 0.30mm^{-2}$. The opened square represents the area selected to calculate the directionality averaged values since (Yellow square) ρ= 0.10 - 0.15mm^{-2} and (Red square) ρ= 0.15 - 0.20mm^{-2}

Individual directionality measurements are possible to obtain with the method at eccentricities larger than 2°. Figure 4(b) (Media 2–Media 5) and Fig. 5(b) (Media 7–Media 10) show images and videos taken at different retinal eccentricities (5°, 10°, 15° and 20° superior parafovea). The positions of a series of cones have been selected randomly across the cone mosaic and the average reflected intensity for each cone has been measured integrating across a circular region with diameter corresponding to 8 pixels (i.e., approximately 4 micron) in each frame. Small movements of the subject's eye change subtle the image location of the cones so that in each case the position of the selected area is shifted manually (frame by frame) tracking the center of the cone analyzed. As shown in Fig. 4(b) and Fig. 5(b) the symbols (■ and ⋆) represent the individual directionalities. The opened squares correspond to the directionality value of the area enclosed by each square.

The individual directionality values range from 0.08 to 0.12mm^{-2} at 2.5° of eccentricity and

#143458 - $15.00 USD Received 1 Mar 2011; revised 21 Apr 2011; accepted 27 Apr 2011; published 4 May 2011

increase approximately three times at 20° where it is expected that cone diameters are similar to the spot size of the incident beam. However, if the directionality is measured for areas across a group of cones the directionality is about 0.14 mm^{-2} (represented by opened squares in Fig. 4(b) and Fig. 5(b)). If the total area of the image is analyzed the directionality is approximately $0.12mm^{-2}$, and approximately constant for different eccentricities.

Figure 6(a) shows the averaged apodization effect of the full images for the subject (BV) for the retinal eccentricities analyzed, where the peak position and the directionality are approximately constant. The peak positions of the apodization effect are approximately equal for both subjects (for simplicity not shown here) and have been reported previously for psychophysical Stiles-Crawford measurements [25].

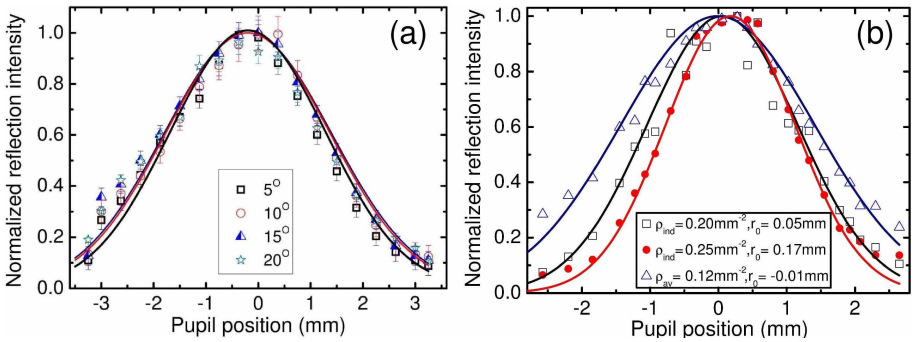

Fig. 6. Reflected average image intensity as a function of pupil entrance point of the imaging beam for the subject BV: (a) total average for superior retinal eccentricities of 5°, 10°, 15°, and 20°, the error values represent the standard deviation; (b) Two examples of individual cone values compared with the value obtained analyzing an area containing the same cones for an eccentricity of 10°, the error values have not been represented such that variations in peak locations can be easily observed.

The difference between the averaged and individual directionality values may plausible be explained by the following reasons: the existence of rods occupying the inter-cone spaces for eccentricies larger than 3 degrees [16], where directionality values are smaller than those of cones [24], and/or a difference in pointing direction for each cone that when averaged creates a broader directionality effect [5]. As shown in Fig. 6(b), the peak position of the apodization effect for individual cones shows a subtle difference of pointing direction that can introduce a broader directionality effect when the area containing the same cones is analyzed.

The directionality values obtained for both subjects at the studied retinal regions are shown in Fig. 7. For the total average values, all the image area is analyzed, and the directionality is obtained for a total of 7 videos. Using the retinal mosaic images at different retinal eccentricities reported by Curcio et al. for ex-vivo human eyes [16] (i.e. from the fovea up to an eccentricity region of 16mm), it is possible to estimate cone diameters at a given eccentricity. A polynomial fitting is used to describe this dependence that by means of Eq. (3) results in the solid line shown in Fig. 7.

In the particular case of Fig. 5(b) (Media 7) the reflection of the blood vessel appear with similar brightness as the cones, indication a non ideal focus on the photoreceptors. For the subject DR it suggests an imperfect conjugation with the confocal pinhole or an incomplete defocus correction. Despite of this, defocus variations are smaller than ΔZ_5=0.05μm that would increase the spot size at the retina plane from 5.2μm to $\approx$ 6-7μm, hence the experimental directionality dependence with eccentricity (solid line in Fig. 7) is still well predicted by use of Eq. (3). Furthermore, it can be noted that the blood vessel reflection has not a directional

#143458 - $15.00 USD Received 1 Mar 2011; revised 21 Apr 2011; accepted 27 Apr 2011; published 4 May 2011

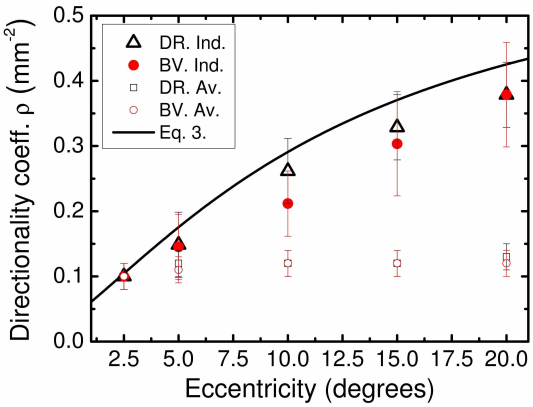

Fig. 7. Individual and total area-averaged directionalities of both subjects at different superior parafoveal eccentricities. The solid line corresponds to the predicted dependence of the directionality coefficient with the eccentricity using Eq. (3) for the special case of $a = w_m$ using the retinal mosaic reported by Curcio et al. [16].

characteristic appearing approximately constant during the pupil scan.

As can be seen in Fig. 5(b) (Media 8, Media 9), there are variations of reflected intensity uncorrelated with the intensity variations of neighboring regions, usually present for a few frames (1-10 frames). The flickering effects can be easier identified for videos at retinal eccentricities larger than 10° and are repeatable for a trial of videos for the same retinal localization. However, most regions with light flash characteristics are smaller than the spatial resolution of our SLO, and the intensity variations have not a well-defined apodization shape. The origin of the effect is not fully understood at present but may be explained for the following reasons: the coherent light illumination is causing the changes either due to rapid index/length variations or local intensity speckles that modulate the coupling efficiency, and/or some cones may have a very narrow acceptance angle because of their composition and geometry.

5. Conclusion

We have demonstrated an SLO imaging method to measure individual cone-photoreceptor directionalities. The method explores the resolution of the SLO system which combined with beam-scan at the pupil allows for a fast and accurate acquisition of the photoreceptor acceptance angle.

As demonstrated by theory and experimental values, the directionality is highly dependent on the light coupling mechanism of the incident beam to the photoreceptor, in this case particularly manifested in the relation between the spot size of the incident beam and the diameter of the photoreceptor. We have observed that although the coupling of the individual cones to the focused incident beam is highly directional a smaller directionality is found when averaged on a larger retinal area.

Acknowledgments

This research was supported by Science Foundation Ireland grants: 07/SK/B1239a and 08/IN.1/B2053 and Enterprise Ireland PC/2008/0125.

#143458 - $15.00 USD Received 1 Mar 2011; revised 21 Apr 2011; accepted 27 Apr 2011; published 4 May 2011